MITSUBISHI ELECTRIC RESEARCH LABORATORIES
http://www.merl.com

Virtual View Synthesis Method and Self Evaluation Metrics for Free Viewpoint Television and 3D Video

Kwan-Jung Oh, Sehoon Yea, Anthony Vetro, Yo-Sung Ho

TR2010-116 December 2010

Abstract

Virtual view synthesis is one of the most important techniques to realize Free viewpoint Tele-Vision (FTV) and Three-Dimensional (3D) video. In this paper, we propose a view synthesis method to generate high quality intermediate views in such applications and new evaluation metrics named as SPSNR and TPSNR to measure spatial and temporal consistency, respectively. The proposed view synthesis method consists of five major steps: depth preprocessing, depth-based 3D warping, depth-based histogram matching, base plus assistant view blending, and depth-based hole-filling. The efficiency of the proposed view synthesis method has been verified by evaluating the quality of synthesized images with various metrics such as Peak Signal-to-Noise Ratio (PSNR), Structural SIMilarity (SSIM), DCT-based Video Quality Metric (VQM), and the newly proposed metrics. We have also confirmed that the synthesized images are objectively and subjectively natural.

International Journal of Imaging Systems and Technology

Virtual View Synthesis Method and Self Evaluation Metrics for Free Viewpoint Television and 3D video

Kwan-Jung Oh, Sehoon Yea, Anthony Vetro, and Yo-Sung Ho

Abstract— **Virtual view synthesis is one of the most important techniques to realize Free viewpoint TeleVision (FTV) and Three-Dimensional (3D) video. In this paper, we propose a view synthesis method to generate high quality intermediate views in such applications and new evaluation metrics named as SPSNR and TPSNR to measure spatial and temporal consistency, respectively. The proposed view synthesis method consists of five major steps: depth preprocessing, depth-based 3D warping, depth-based histogram matching, base plus assistant view blending, and depth-based hole-filling. The efficiency of the proposed view synthesis method has been verified by evaluating the quality of synthesized images with various metrics such as Peak Signal-to-Noise Ratio (PSNR), Structural SIMilarity (SSIM), DCT-based Video Quality Metric (VQM), and the newly proposed metrics. We have also confirmed that the synthesized images are objectively and subjectively natural.**

Index Terms—**View synthesis, free viewpoint television (FTV), 3D video, image-based rendering (IBR), evaluation of virtual view**

I. Introduction

Three-Dimensional (3D) video provides users with a realistic 3D impression of the scene and is now considered a key technology that could spur the next wave of multimedia experiences such as 3D cinema, 3D broadcasting, 3D displays, and 3D mobile services [1]-[4].

The key technical building blocks of the 3D processing chain are coding and rendering. The role of efficient coding becomes much more important for 3D systems due to the drastic increase in the volume of data. Some of the past research and standardization efforts to address this issue include MPEG-2 Multiview Video Profile (MVP) [5], MPEG-4 Multiple Auxiliary Component (MAC) [6], and MPEG/JVT Multiview Video Coding (MVC) [7]-[12]. Recently, MPEG has initiated a work aimed specifically towards 3D video applications. While the previous MPEG/JVT standardization activities for MVC was focused on compression efficiency improvement for generic multiview coding scenarios, this activity will target a broader technical scope including issues such as depth estimation, coding, and rendering. One of the current underlying key design assumptions is the use of depth maps along with camera parameters for rendering intermediate views for either free viewpoint navigation or 3D displays.

On the other hand, given the ever increasing diversity in 3D services and displays, proper rendering of 3D views is indispensable. In other words, it becomes necessary to resample the views and resize each view depending on the number of views and resolutions required by the display, respectively. For applications such as FTV [13]-[15] and the case when there are more views to be rendered at the display than are actually coded, resampling means generation of virtual views based upon the actual views. The problem of generating an arbitrary view of a 3D scene has been heavily addressed in the area of computer graphics. Among the techniques for rendering, Image-Based Rendering (IBR) techniques have received much attention lately for rendering real world scenes. These techniques use image rather than geometry as primitives for rendering virtual views and often are classified into three categories depending on how much geometric information is used [16]: rendering without geometry, with explicit geometry, and with implicit geometry. Techniques such as plenoptic modeling [17], light-field rendering [18], lumigraph [19], and ray-space [20], [21] belong to the rendering without geometry. In this approach, the quality of view synthesis usually depends on the baseline distance and the synthesis quality increases with the number of available views within a restricted viewing angle. On the other hand, an IBR system with depth maps which uses techniques such as 3D warping and Layered-Depth-Images (LDIs) belongs to the second category while view morphing and view interpolation as in [22]-[27] belong to the third category as they use the point correspondences. Obviously the quality of view synthesis in these explicit/implicit geometry-based rendering approaches largely depends on the accuracy of the geometry information.

In this paper, we propose a new view synthesis algorithm within the aforementioned scope of the FTV and 3D video activities [28] and new evaluation metrics to measure the spatial and temporal consistencies of the synthesized views. The proposed view synthesis method consists of five major steps: depth preprocessing, depth-based 3D warping, depth-based histogram matching, base plus assistant view blending, and depth-based hole-filling. First, a preprocessing is performed on the acquired scene depth data in order to correct errors and enhance the spatial and temporal consistencies of depth values. Second, a depth-based 3D warping technique is adopted to avoid the discontinuity problem in the direct warping of textures caused by round-off errors. Third, a depth-based histogram matching algorithm is employed to reduce the illumination difference between two reference views. Fourth, a base plus assistant view blending is introduced to blend two 3D warped reference images in a robust manner against the inaccuracy of the depth and camera parameters. Finally, a depth-based hole-filling technique is used to fill the remaining holes using a depth-based in-painting technique. The synthesized view is evaluated by Peak Signal-to-Noise Ratio (PSNR), Structural SIMilarity (SSIM) [29], DCT-based Video Quality Metric (VQM) [30] [31], and the newly proposed spatial PSNR (SPSNR) and temporal PSNR (TPSNR).

The rest of this paper is organized as follows. In Section 2, we describe the basics of view synthesis. We explain the details of the proposed view synthesis algorithm and the evaluation metrics in Sections 3 and 4, respectively. We then demonstrate and evaluate the performance of the proposed scheme in Section 5, and conclude the paper in Section 6.

II. Background

This section briefly reviews the camera geometry model and the general idea of depth-based view synthesis.

A. Camera Geometry Model

A general pinhole camera is modeled by its *optical center C* and its *image plane I*. A 3D point *W* is projected into an image point *M* given by the intersection of *I* with the line containing *C* and *W*. The line containing *C* and orthogonal to *I* is called the *optical axis* (*Z*) and its intersection with *I* is the *principal point* (*p*). The distance between *C* and *I* is the *focal length*.

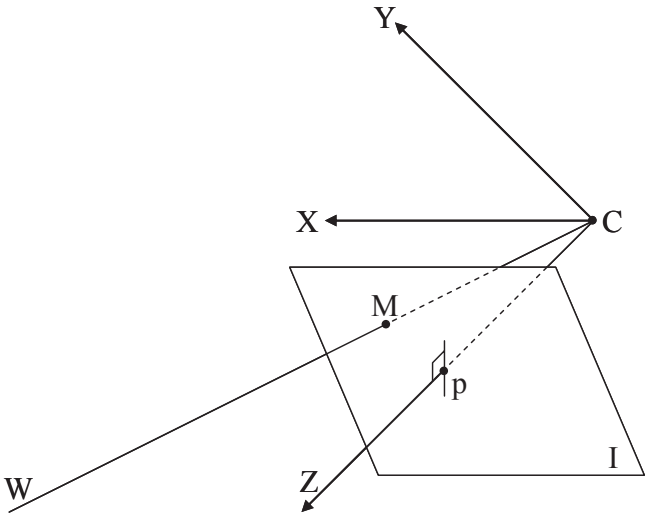

Fig. 1. The pinhole camera model

Let $w = [x\ y\ z]^T$ be the coordinates of *W* in the world reference frame (fixed arbitrarily) and $m = [u\ v]^T$ the coordinates of *M* in the image plane (pixels). The mapping from 3D coordinates to 2D coordinates is *perspective projection*, which is represented by a linear transformation in *homogeneous coordinates*. Let $\tilde{m} = [u\ v\ 1]^T$ and $\tilde{w} = [x\ y\ z\ 1]^T$ be the homogeneous coordinates of *M* and *W*, respectively; then, the perspective transformation is given by the matrix $\tilde{P}$:

$$\kappa\tilde{m} = \tilde{P}\tilde{w}, \tag{1}$$

where κ is a scale factor called *projective depth*. κ becomes the true orthogonal distance of the point from the focal plane of the camera. The camera is therefore modeled by its *perspective projection matrix* (henceforth simply *camera matrix*) $\tilde{P}$, which can be decomposed, using the QR factorization, into the product

$$\tilde{P} = A[R \mid t]. \tag{2}$$

The matrix A depends on the *intrinsic parameters* only, and has the following form:

$$A = \begin{bmatrix} \alpha_u & \gamma & u_0 \\ 0 & \alpha_v & v_0 \\ 0 & 0 & 1 \end{bmatrix}, \tag{3}$$

where $\alpha_u = -fk_u$, $\alpha_v = -fk_v$ are the focal lengths in horizontal and vertical pixels, respectively (f is the focal length in millimeters, k_u and k_v are the effective number of pixels per millimeter along the u and v axes), (u_0, v_0) is the coordinate of the *principal point* given by the intersection of the optical axis with the retinal plane as shown in Fig. 1, and γ is the skew factor that models non-orthogonal $u - v$ axes.

The camera position and orientation (*extrinsic parameters*) are represented by the 3 x 3 rotation matrix R and the translation vector t , respectively, corresponding to the rigid transformation that brings the camera reference frame onto the world reference frame [32]-[34].

B. Depth-based View Synthesis

The schematic diagram of a typical depth-based view synthesis system is shown in Fig. 2. The goal of such a system is to synthesize a virtual view from its neighboring views using the camera parameters, texture images, and depth images.

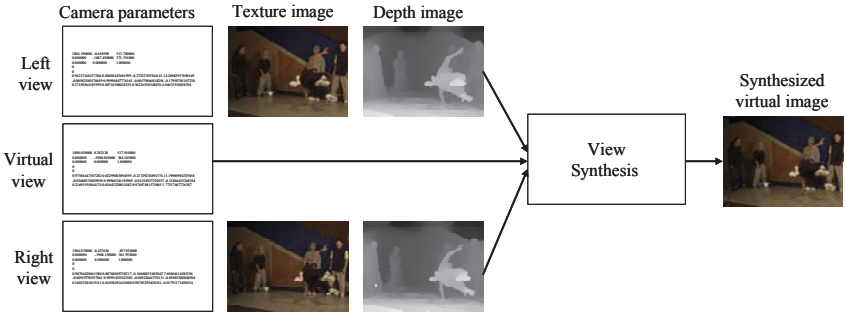

Fig. 2. Depth-based virtual view synthesis

The Three-Dimensional image warping (3D warping) is the key technique in depth-based view synthesis. In 3D warping, pixels in the reference image are back-projected to 3D spaces, and re-projected onto the target viewpoint as shown in Fig. 3.

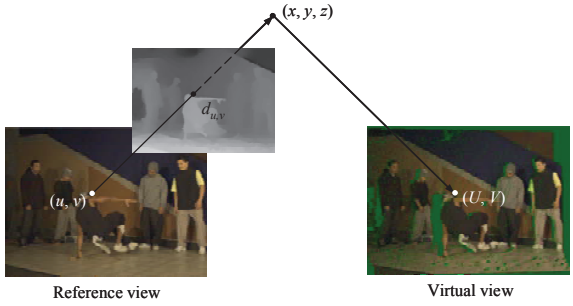

Fig. 3. General concept of 3D warping

Equations (4) and (5) represent the back-projection and the re-projection processes, respectively.

$$(x, y, z)^T = R_{ref} A_{ref}^{-1} (u, v, 1)^T d_{u,v} + t_{ref} \tag{4}$$

$$(l, m, n)^T = A_{vir} R_{vir}^{-1} \{(x, y, z)^T - t_{vir}\} \tag{5}$$

where A, R, and t are camera parameters and d represents the depth value of a point in the 3D space that needs to be back-/re-projected. The coordinate (l, m, n) in (5) is normalized to (l/n, m/n, 1) and then represented as an integer-coordinate (U, V) in the virtual view.

III. Proposed View Synthesis Algorithm

The proposed view synthesis algorithm consists of five steps: depth preprocessing, depth-based 3D warping, depth-based histogram matching, base plus assistant view blending, and depth-based hole-filling. Fig. 4 shows a diagram of the proposed view synthesis scheme and each sub-algorithm will be detailed in the following subsections.

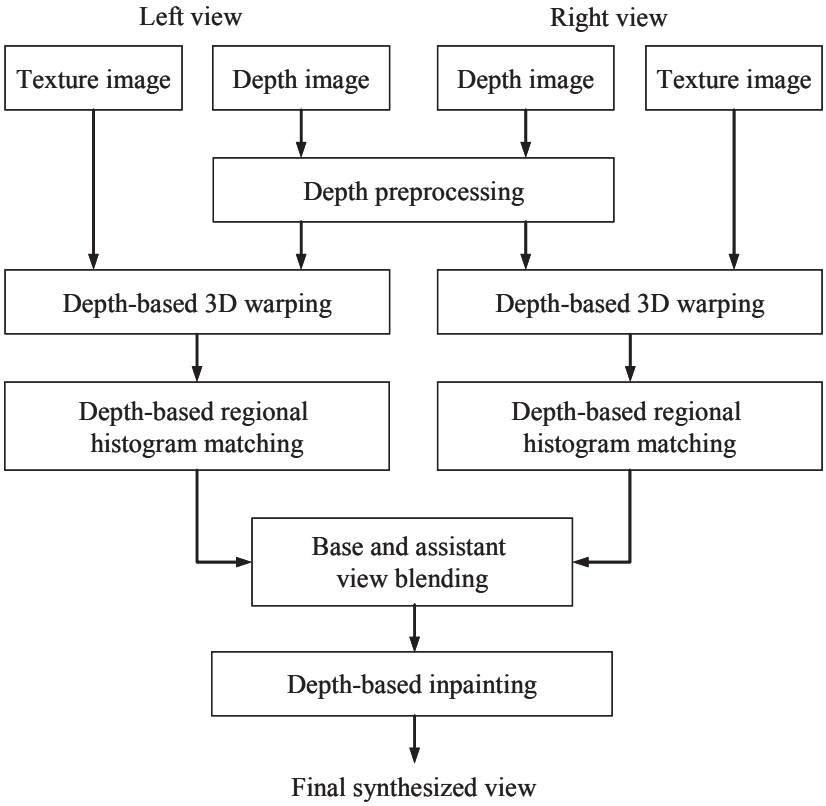

Fig. 4. Diagram of the proposed view synthesis scheme

A. Depth Preprocessing

In general, the depth data can be obtained by a special depth camera system and computer graphics tools or mathematically calculated by depth estimation algorithms. Currently depth estimation is the most popular approach and actively studied since the depth camera is too expensive and computer graphic images cannot represent real scenes.

However, mathematically calculated depth data tend to have erroneous values in certain regions in the image or have inconsistent values across spatial or temporal neighbors due to the local nature of depth-estimation process. These problems associated with depth could lead to various visual artifacts in the synthesized images. To resolve these issues, we propose to preprocess the depth data. The proposed depth preprocessing consists of three steps: temporal filtering, initial error compensation, and spatial filtering. Basically we apply a median filtering instead of averaging filter because averaging filter results in new pixel values which do not exist in the initial depth image, which degrades rendering quality.

As a first step, we apply a 1D median filter along the co-located pixels of consecutive depth image frames. It aims to reduce the temporal inconsistency of depth values belonging to the same object or background. In this paper, we apply a median filter as follows:

$$Y_{i,j,t} = \begin{cases} median(J_{i,j,t}), & for \quad max(J_{i,j,t}) - min(J_{i,j,t}) <= \gamma \\ X_{i,j,t}, & otherwise \end{cases} \tag{6}$$

where $X_{i,j,t}$ is the value of a pixel at the spatial location (i, j) at time t, $J_{i,j,t}$ is a set of pixels in a 3×3 window centered around the spatio-temporal location (i, j, t), and γ is a threshold value to determine whether or not the filter will be applied.

The next step has to do with compensating for the initial error which is caused by an erroneous merge of foreground and background in the typical depth estimation process. Usually, it occurs when the foreground and the background have similar textures. The human eyes can easily distinguish them but it is often a difficult task for an automated algorithm. In this paper, we correct the initial errors by using image dilation and erosion as in (7) and (8) respectively [35]. Since the quality of a synthesized image will be worse in case the foreground has a background's depth value than the other way around, image dilation is conducted prior to image erosion in the proposed scheme.

$$A \oplus B(x,y) = \max_{(x,y)\in B} \left[A_B(x,y) \right] \tag{7}$$

$$A \ominus B(x,y) = \min_{(x,y)\in B} \left[A_B(x,y) \right] \tag{8}$$

where A represents the image and B is structuring element which operates on the A. The A_B is a masked region with B and (x, y) is a pixel in the image A. In this paper, we use a disk-shaped structuring element with disk radius set to five.

The final step has to do with smoothing outliers in an estimated depth image using a 2D median filter. It smoothes out the outlier of objects in a depth image and removes the unwanted noises. In this paper, we employ a 5×5 median filter for every pixel at (i, j) as follows:

$$Y_{i,j} = median(J_{i,j}) \tag{9}$$

where $J_{i,j}$ is a set of pixels in a 5×5 window centered around the location (i, j).

Fig. 5 illustrates the result of each step of the proposed depth-preprocessing for "Breakdancers" provided by MicroSoft Research (MSR) [36]. The effect of the proposed scheme is noticeable especially around the faces of the two men standing behind on the left side of the dancer as well as around the boundaries of the dancer on the floor. The proposed depth preprocessing method

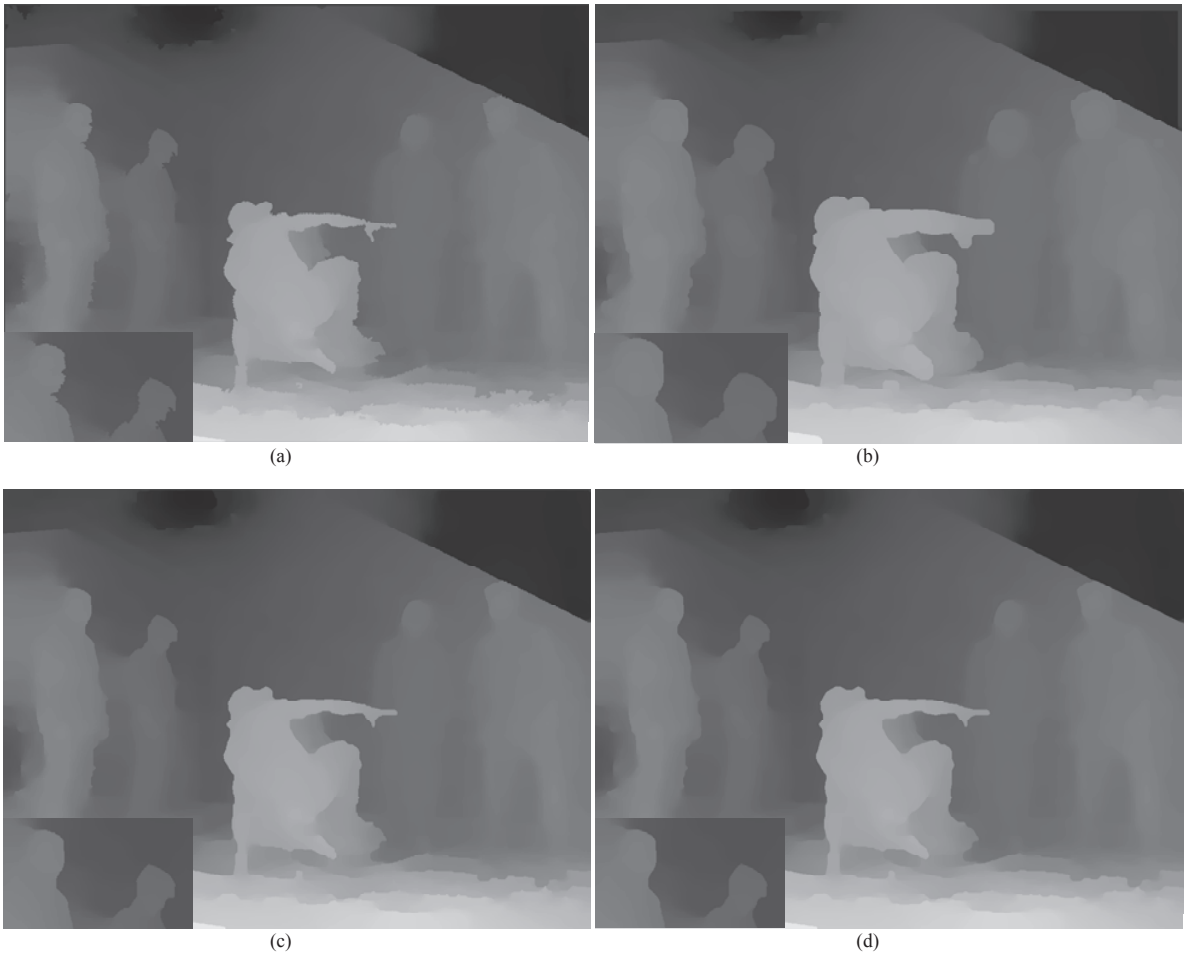

Fig. 5. An example of depth-preprocessing for "Breakdancers" sequence: (a) temporal filtered image (b) dilated image (c) eroded image (d) spatial filtered image

not only compensates for the initial depth errors efficiently, but also recovers the spatial and temporal consistency [37]. Hence the preprocessed depth will lead to significantly improved objective and subjective qualities of the synthesized images.

B. Depth-based 3D Warping

Most previous view synthesis algorithms warp the texture images using the corresponding depth maps. However, a direct 3D warping of texture images of neighboring views into the virtual image plane often causes false black-contours in the synthesized image as shown in Fig. 6 (b). These contours are caused by round-off errors involved with the integer representation of the virtual view's coordinate as well as by spurious initial depth values.

(a) (b)

Fig. 6. 3D warping with erroneous blanks: (a) depth image, (b) 3D warped texture image using (a)

However, once the depth image corresponding to the virtual view is obtained, we can use it to always find, by inverse warping, the proper texture values from its neighboring view without generating false black-contours in the synthesized view. In order to obtain the depth image corresponding to the virtual view, we first warp the depth values of the reference view. Note that the false black-contours appear in the warped depth image as shown in Fig. 7 (a) for the exactly same reason as with the texture warping. In order to remove these erroneous contours, we apply a median filtering [38]. Fig. 7 illustrates the above procedures.

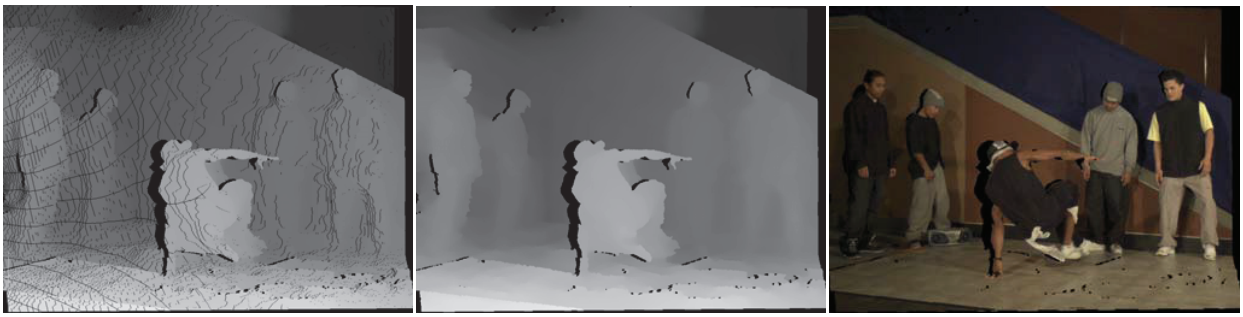

(a) (b) (c)

Fig. 7. 3D warping without erroneous blanks: (a) 3D warped depth image, (b) median filtered depth for (a), (c) 3D warped texture image using (b)

C. Depth-based Histogram Matching

In case we have two reference views for the virtual view synthesis as shown in Fig. 2, we can first synthesize two 3D warped views, i.e., one from each view. Before blending these two warped images, we apply a histogram matching to reduce the illumination and color differences between the two images which may cause inconsistency of the synthesized image. Based on previous histogram matching algorithm [39], we modify the mapping condition considering the distributions of cumulative histograms and then apply this modified histogram matching regionally using depth-based segments.

The histograms of the two 3D warped images for reference views are analyzed and those 3D warped images are adjusted to have a similar distribution. The whole procedures of histogram matching are as follows. The first step is to modify the two 3D warped images to have same holes and then to apply a median filter for noise reduction as shown in Fig. 8. By using the modified images instead of original 3D warped images, the accuracy of the histogram matching is improved.

Fig. 8. Image modification for histogram matching: (a) 3D warped view 3, (b) 3D warped view 5, (c) modified view 3, (d) modified view 5

The second step is to compute the histograms of the left image and the right image. Let $y_L[m,n]$ denote the amplitude of the left image. Then its histogram is given as follows:

$$h_L[v] = \frac{1}{w \cdot h} \sum_{m=0}^{h-1} \sum_{n=0}^{w-1} \delta[v, y_L[m,n]] \qquad (10)$$

$$with \quad \delta[a,b] = \begin{cases} 1 & , \text{ if } a = b \\ 0 & , \text{otherwise} \end{cases}$$

In (10), w denotes the image width and h is the image height. The value of v ranges from 0 to 255. The histogram matching is done by mapping the left and right images to a virtual image. Two steps are necessary to generate the mapping function M. First, the cumulative histogram $C_L[v]$ of the left image is created:

$$C_L[v] = \sum_{i=0}^{v} h_L[i] \qquad (11)$$

The histogram $h_R[v]$ and cumulative histogram $C_R[v]$ of the right image are calculated in the same manner. Both the left and right images, which are already warped into the virtual view position, are median-filtered and modified to have the same holes as shown in Fig. 8 (c) and (d) so that the two views have almost identical textures except for slight differences in their illuminations.

Based on the cumulative histograms, we make a cumulative histogram $C_V[v]$ for virtual:

$$C_V(v) = \alpha\ C_L(v) + (1-\alpha)C_R(v) \tag{12}$$

where C_L and C_R are the cumulative histograms for left and right images. Generally, the weighting factor α is calculated based on the baseline distance as follows:

$$\alpha = \frac{|t_V - t_L|}{|t_V - t_L| + |t_V - t_R|} \tag{13}$$

where t is a translation vector for each view.

The mapping function between the left image and the virtual image is obtained by matching the number of occurrences in the reference image to that of occurrences in the virtual image as in (14) and as shown in Fig. 9 as an example.

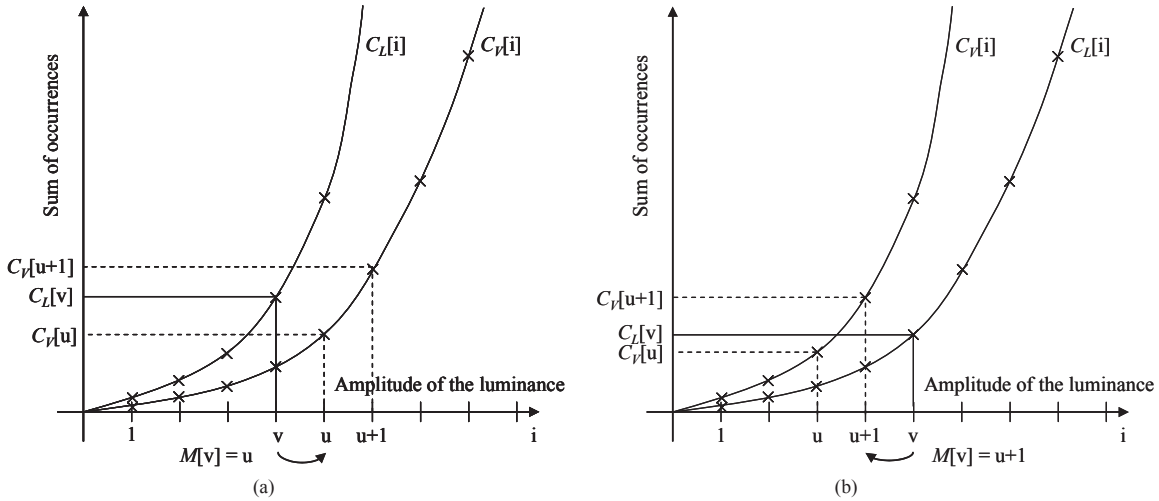

Fig. 9. Mapping algorithm using cumulative histograms: (a) $C_V[v] <= C_L[v]$, (b) $C_V[v] > C_L[v]$,

$$M[v] = \begin{cases} u, & for \quad C_V[u] < C_L[v] \le C_V[u+1] \;\; \& \;\; C_V[v] <= C_L[v] \\ u+1, & for \quad C_V[u] < C_L[v] \le C_V[u+1] \;\; \& \;\; C_V[v] > C_L[v] \end{cases} \tag{14}$$

The calculated mapping function is applied to the left image $y_L[m, n]$, resulting in the histogram-matched image $y_{HML}[m, n]$ as in (15). The histogram $y_{HMR}[m, n]$ of the right image is calculated in the same manner.

$$y_{HML}[m,\ n] = M[y_L[m,\ n]] \tag{15}$$

In general, we assume that the difference of volume of light for each camera causes the illumination and color differences and differently affects each object and color component. By considering the above assumption, we apply the histogram matching regionally and the regions are divided using depth. Fig. 10 shows an example of rough region division for the image in Fig. 8 (d).

While the previous histogram matching converts one view to the other to have a similar histogram, the proposed histogram matching modifies the both views to have similar histogram as that of the virtual view which is defined by considering baseline distances. In addition, the proposed histogram matching maps the indices differently for the two cases in Fig. 9.

(a) (b)

Fig. 10. Rough region division by depth: (a) foreground region, (b) background region

Fig. 11 shows an example for proposed histogram matching. In this case, histograms of the 3D warped left and right views have similar shapes but different distributions caused by illumination and color differences. By mapping these two reference view to have a similar cumulative histogram with that of the virtual view, we can reduce the illumination differences between two views. The proposed histogram matching is independently applied to each color component of RGB format.

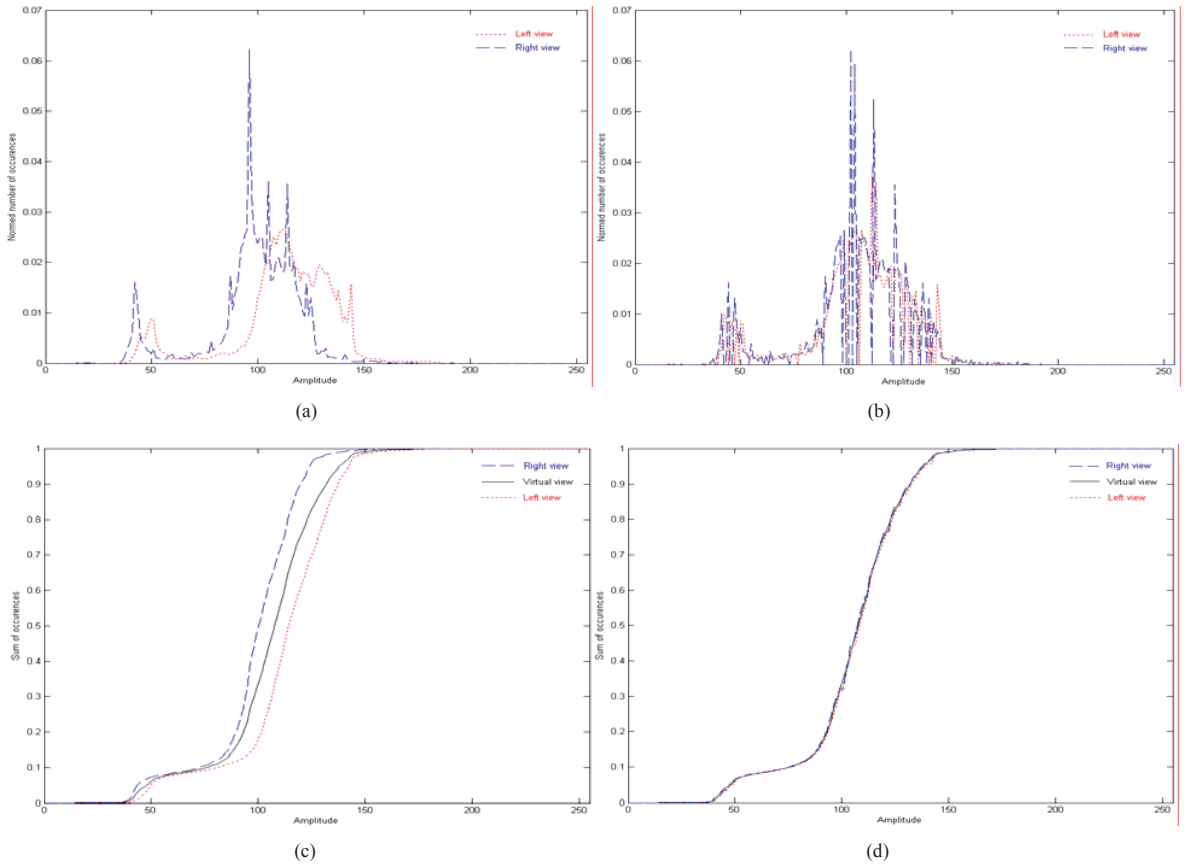

Fig. 11. Histogram matching: (a) histograms (b) histograms after histogram matching (c) cumulative histograms (d) cumulative histograms after histogram matching

D. Base plus Assistant View Blending

The boundary errors around the big holes are usually caused by inaccuracy of the camera parameters and inaccurate boundary matching between texture images and depth images. To remove these visible errors we extend the hole boundaries by using image dilation as shown in Fig. 12. These extended holes can be filled by the other 3D warped view and we expect more natural synthesized view by removing this kind of errors.

The next step is view blending to combine 3D warped views to the virtual view and the simplest way would be taking a weighted sum of the two images as below:

$$I_V(u,v) = \alpha\ I_L(u,v) + (1-\alpha) I_R(u,v) \tag{16}$$

where I_L and I_R are the 3D warped reference texture images and I_V is an image to be blended. Generally, the weighting factor α is calculated based on the baseline distance as in (13).

(a) (b)

Fig. 12. Hole extension: (a) before extension (b) after extension

However, a drawback of this method is that inconsistent (due to, for e.g., camera parameters, inconsistent depth values etc.) pixel values from both views can contribute to the warped image and often leads to an unnaturalness such as double edge artifacts and smoothing as shown in Fig. 13. In order to avoid such a problem, we define a base view and an assistant view for view blending. The base view is the main reference view from which most of the pixel values are warped, and the assistant view is used as a supplementary reference view for hole-filling. Then (16) can be rewritten as (17), where α is 1 for non-hole regions and 0 for hole regions in the 3D warped base view. In other words, most regions of the blended view come from the base view and some remaining holes are filled from the assistant view. We choose a closer view from the virtual view as the base view.

$$I_V(u,v) = \alpha\ I_B(u,v) + (1-\alpha) I_A(u,v) \tag{17}$$

where I_B is the base view and I_A is the assistant view.

(a) (b)

Fig. 13. View blending methods: (a) weighted sum method (b) base and assistant method

E. Hole-Filling using Depth-based In-painting

The last step of the proposed view synthesis is depth-based hole-filling. Even though view blending efficiently fills up most disoccluded regions, some holes still remain. In general, these remaining holes are caused by still remaing disocclusion regions and wrong depth value. Disocclusion regions are defined as areas that cannot be seen in the reference image, but exist in the synthesized one. Many existing hole-filling methods use image interpolation or in-painting techniques and fill up the remaining holes using neighboring pixels solely based upon geometrical distance. However, observe that it make more sense to fill up the holes using the background pixels rather than the foreground ones as the disoccluded area usually belongs to the background by definition. Therefore we propose a hole-filling algorithm which prefers the background pixels over the foreground ones in addition to considering the existing in-painting technique.

The general in-painting problem is as follow [40]: the region to be in-painted Ω and its boundary $\partial\Omega$ are defined and the pixel p belong to Ω would be in-painted by its neighboring region $B_\varepsilon(p)$ as shown in Fig. 14 .

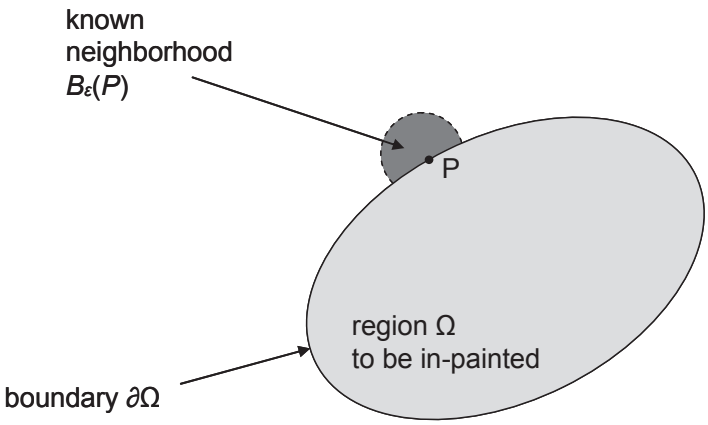

Fig. 14. General in-painting circumstance

This concept is quite reasonable for common image in-painting but it should be changed to be applied to hole-filling in view synthesis because $\partial\Omega$ of a certain hole can belong to both the foreground and the background. In this case, we replace the boundary region facing the foreground with the corresponding background region located on the opposite side as depicted in (18). That is, we intentionally manipulate the hole to have neighborhood belonging only to the background as shown in Fig. 15.

$$\begin{aligned} p_{fg} \in \partial\Omega_{fg} &\rightarrow p_{bg} \in \partial\Omega_{bg} \\ B_\varepsilon(p_{fg}) &\rightarrow B_\varepsilon(p_{bg}) \end{aligned} \tag{18}$$

where *fg* and *bg* represent the foreground and the background, respectively.

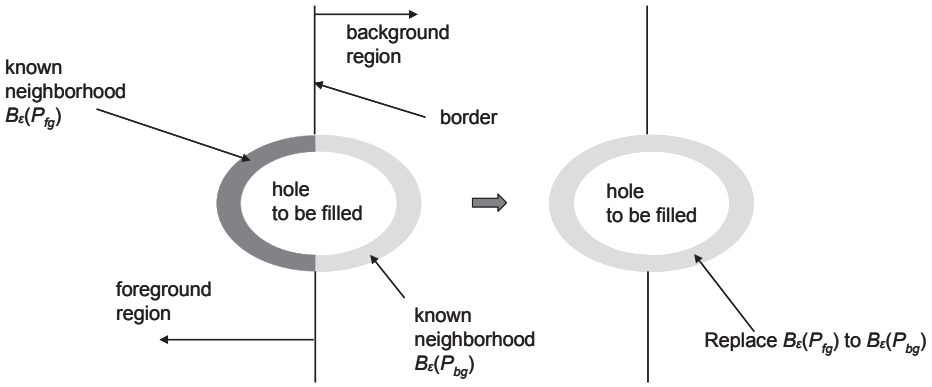

Fig. 15. Manipulation of hole to have neighborhood only come from background

To distinguish the foreground and the background, we use the corresponding depth data. In other words, for the two pixels horizontally opposite to each other on the hole boundary, we regard the pixel having the larger depth value as belonging to the foreground and vice versa. Fig. 16 shows the results from the previous in-painting and the proposed depth-based in-painting techniques.

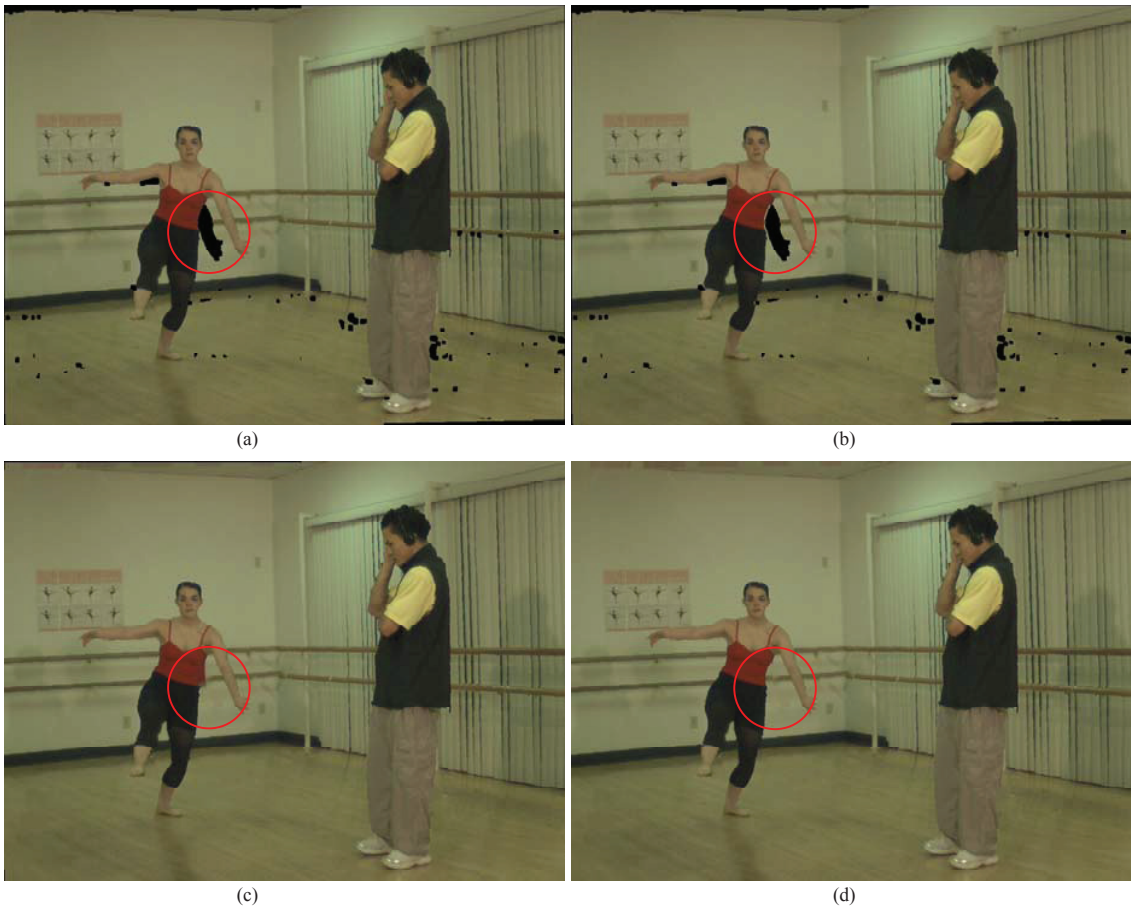

Fig. 16. In-painting procedure: (a) image with holes, (b) boundary region copy from background, (c) previous in-painting, (d) proposed depth based in-painting

IV. Self Evaluation Metrics

To evaluate the performance of the view synthesis algorithm, generally we measure the similarity between the synthesized view and the existing original one. The PSNR, SSIM [29], and VQM [30] are widely used but these are only useful when the original view is available for virtual view. In addition, they cannot evaluate temporal consistency which is susceptible to illumination changes and the focus-mismatch and to which human eyes are quite sensitive.

In order to overcome the limitations of the existing evaluation measure, we propose new evaluation metrics named as Spatial PSNR (SPSNR) and Temporal PSNR (TPSNR). The SPSNR measure the spatial consistency by checking spatial noise caused by view synthesis. Generally, the view synthesis increases the high frequency components since the 3D warped images and holes have a lot of high frequency component. Thus, we can evaluate the spatial consistency by checking the degree of the volume of the increased high frequency components. From the above concept, the S-PSNR is defined as follows :

$$
\begin{aligned}
SPSNR &= 10\log\frac{255^2}{SMSE} \\
SMSE &= \frac{1}{h\times w}\sum_{i=1}^{w}\sum_{j=1}^{h}\left[img(i,j)-img_{LPF}(i,j)\right]^2
\end{aligned}
\tag{19}
$$

where h and w denote image height and width. We apply the 5×5 median filter as a LPF to remove spatial noise and its difference image with the original image only contains the high frequency components. We define the volume of the high frequency components as SMSE similar to MSE in PSNR and develop the SPSNR similar to existing PSNR.

The TSPNR to evaluate the temporal consistency is similar with the SPSNR except for its input image is replaced with the difference image between two temporally successive frames in (20). The TPSNR measure the high frequency components of the temporal changes. The main merit of the proposed measures is it only uses the synthesized view itself.

$$
\begin{aligned}
TPSNR &= 10\log\frac{255^2}{TMSE} \\
TMSE &= \frac{1}{h\times w}\sum_{i=1}^{w}\sum_{j=1}^{h}\left[imgD(i,j)-imgD_{LPF}(i,j)\right]^2 \\
imgD(t) &= \left|img(t)-img(t-1)\right|
\end{aligned}
\tag{20}
$$

V. Experimental Results and Analysis

We have tested the proposed algorithm on two test sequences: “Breakdancers” and “Ballet”. Among the 8 views, view 3 and view 5 were selected as reference views and view 4 is set as the virtual view to be synthesized. Each major sub-algorithm of the proposed method is evaluated by existing objective evaluation measures, such as PSNR, SSIM [29], VQM [30], and the proposed SPSNR and TPSNR. While a larger value means a better quality for PSNR, SPSNR, and TPSNR, the opposite is ture for VQM. In the case of SSIM, the closer the value is to 1, the better is the quality. The proposed view synthesis algorithm was compared to the view synthesis software version 2.3 [41] released by Nagoya University which is currently used as a reference software in MPEG FTV/3D video standardization activity. The default view blending method in the reference SW was replaced with the proposed base plus assistant method to make a more meaningful comparison.

A. Experimental Results for Depth Preprocessing

The results for depth preprocessing are given in Table I and their corresponding samples of synthesized images are shown in Fig. 17. The depth preprocessing does not provide noticeable quality improvements in terms of the existing evaluation measures, but it shows some gains for SPSNR and TPSNR. Especially, we can confirm that the temporal consistency of the “Ballet” sequence is enhanced by depth preprocessing. In addition, we can confirm some improvements such as natural smooth boundary for the dancer on the floor and the shapes of the heads of the two dancers standing on the left.

TABLE I
Experimental Results for “Depth Preprocessing”

Evaluation Measures	Breakdancers		Ballet	
	without preprocessing	with preprocessing	without preprocessing	with preprocessing
PSNR	31.7300	31.6421	31.7773	31.7935
SSIM	0.8381	0.8379	0.8736	0.8739
VQM	3.9973	4.0984	2.6134	2.5351
SPSNR	38.8363	38.9236	38.3793	38.5004
TPSNR	37.8345	38.0415	39.6727	40.7091

(a) (b)

Fig. 17. Synthesized images: (a) without depth preprocessing (b) with preprocessing

B. *Experimental Results for Depth-based Histogram Matching*

As shown in Table II and sample images in Fig. 18, the proposed histogram matching improves the subjective quality by reducing the illumination and color changes. However, its objective quality is slightly degraded.

TABLE II
EXPERIMENTAL RESULTS FOR "HISTOGRAM MATCHING"

Evaluation Measures	Breakdancers		Ballet	
	without histogram matching	with histogram matching	without histogram matching	with histogram matching
PSNR	31.7300	31.8754	31.7773	31.5912
SSIM	0.8381	0.8367	0.8736	0.8714
VQM	3.9973	3.9729	2.6134	2.7049
SPSNR	38.8363	38.7442	38.3793	38.0913
TPSNR	37.8345	37.7891	39.6727	39.5653

(a) (b)

Fig. 18. Histogram matching: (a) without histogram matching, (b) with histogram matching

C. *Experimental Results for Proposed Depth-based In-painting*

The experimental results for depth based in-painting are given in Table III and their corresponding synthesized sample images are in Fig. 19. The proposed depth-based in-painting fills up the remaining holes using only the pixels located in the background when the holes border with both the foreground and the background. We can confirm the proposed method improves both the subjective and the objective qualities.

TABLE III
EXPERIMENTAL RESULTS FOR "HOLE FILLING USING IN-PAINTING"

Evaluation Measures	Breakdancers		Ballet	
	previous in-painting	depth-based in-painting	previous in-painting	depth-based in-painting
PSNR	31.7300	31.7484	31.7773	32.4967
SSIM	0.8381	0.8384	0.8736	0.8740
VQM	3.9973	3.9852	2.6134	2.5131
SPSNR	38.8363	38.8448	38.3793	38.3821
TPSNR	37.8345	37.8458	39.6727	39.8938

(a) (b)

Fig. 19. In-painting: (a) previous in-painting (b) depth-based in-painting

D. Experimental Results for the Proposed View Synthesis Method

The proposed view synthesis method consists of various sub algorithms such as depth preprocessing, depth-based 3D warping, depth-based histogram matching, base and assistant view blending, and hole-filling using depth-based in-painting. In this section, the proposed view synthesis method is compared to the reference view synthesis software [41]. The main tools of the reference software are depth-based 3D warping, hole-filling using in-painting, and weighted sum based view blending. In this experiment, we replace the view blending method in reference view synthesis software with the base plus assistant method.

The experimental results are given in Table IV and their corresponding synthesized sample images in Fig. 20 and Fig. 21. We could confirm that the synthesized images by the proposed view synthesis method is both subjectively and objectively better than those of the reference software.

TABLE IV
EXPERIMENTAL RESULTS FOR "PROPOSED VIEW SYNTHESIS METHOD"

Evaluation Measures	Breakdancers		Ballet	
	reference software	proposed method	reference software	proposed method
PSNR	31.6292	31.8150	32.1825	32.2854
SSIM	0.8341	0.8365	0.8664	0.8718
VQM	3.9273	4.0628	2.7430	2.5351
SPSNR	38.4073	38.8319	37.8048	38.2107
TPSNR	37.3941	38.0104	39.2467	40.6742

(a) (b)

Fig. 20. Synthesized images for “Breakdancers” sequence: (a) reference software (b) proposed method

(a) (b)

Fig. 21. Synthesized images for “Ballet” sequence: (a) reference software (b) proposed method

VI. Conclusions

In this paper, we have proposed a virtual view synthesis method and self evaluation metrics for FTV and 3D video. The proposed method consists of four steps : depth preprocessing, depth-based 3D warping, illumination and color difference compensation with a depth-based histogram matching, and hole filling by a depth-based in-painting technique. In addition, a base plus assistant view blending method was introduced for better subjective quality compared to the weighted-sum based view blending. The effectiveness of the proposed method was confirmed by evaluating the quality of the synthesized image using various quality measures including the newly proposed self-evaluation metrics SPSNR and TPSNR. We observed that the proposed method produced both subjectively and objectively better results compared with those by the current reference software being used in the MPEG FTV/3D video standardization activities.

REFERENCES

[1] M. Tanimoto, "Overview of free viewpoint television," *Proc. of Signal Processing: Image Communication*, vol. 21, pp. 454–461, July 2006.

[2] A. Smolic and P. Kauff, "Interactive 3D video representation and coding technologies," *Proc. of IEEE, Special Issue on Advances in Video Coding and Delivery*. vol. 93, pp. 99–110, 2005.

[3] M. Tanimoto, "Free viewpoint television - FTV," *Picture Coding Symposium (PCS 2004)*, Session 5, Dec. 2004.

[4] F.Isgro, E. Trucco, P. Kauff, and O. Schreer, "3D image processing in the future of immersive media," *Proc. of IEEE Transactions on Circuits and Systems for Video Technology*, vol.14, no. 3, pp. 288–303, 2004.

[5] X. Chen and A. Luthra, "MPEG-2 multiview profile and its application in 3D TV," *Proc. of SPIE-Multimedia Hardware Architectures*, vol. 3021, pp. 212–223, 1997.

[6] H. A. Karim, S. Worrall, A. H. Sadka, and A. M. Kondoz, "3D video compression using MPEG-4-multiple auxiliary component (MPEG4-MAC)," *Proc. of IEE 2nd International Conference on Visual Information Engineering (VIE2005)*, Apr. 2005.

[7] ISO/IEC JTC1/SC29/WG11, "Requirements and application descriptions on multi-view video coding," Doc. N9543, Oct. 2007.

[8] A. Smolic and D. McCutchen, "3DAV exploration of video-based rendering technology in MPEG," *Proc. of IEEE Transactions on Circuit and System for Video Technology*, vol. 14, no. 3, pp. 348–356, Mar. 2004.

[9] A. Smolic, H. Kimata, and A.Vetro, "Development of MPEG standards for 3D and free viewpoint video," *Proc. of SPIE Optics East, Three-Dimensional TV, Video, and Display IV*, Boston, MA, Oct. 2005.

[10] ISO/IEC JTC1/SC29/WG11, "Call for comments on 3DAV," Doc. N6051, Oct. 2003.

[11] ISO/IEC JTC1/SC29/WG11, "Survey of algorithms used for multi-view video coding (MVC)," Doc. N6909, Jan. 2005.

[12] H.Y. Shum, J. Sun, S. Yamazaki, Y. Lin, and C.K. Tang, "Pop-up light field: An interactive image-based modeling and rendering system," *Proc. of SIGGRAPH (ACM Trans. Graphics)*, vol. 23, no. 2, pp. 143–162, Apr. 2004.

[13] C.L. Zitnick, S.B. Kang, M. Uyttendaele, S. Winder, and R. Szeliski, "High-quality video view interpolation using a layered representation," *Proc. of SIGGRAPH (ACM Trans. Graphics)*, pp. 600–608, Aug. 2004.

[14] Z.F. Gan, S.C. Chan, K.T. Ng, and H.Y. Shum, "An object-based approach to plenoptic videos," *Proc. of International Symposium on Circuits and Systems (ISCAS2005)*, pp.3435–3438, May 2005.

[15] J. Shade, S. Gortler, L.W. He, and R. Szeliski, "Layered depth images," *Proc. of SIGGRAPH (ACM Trans. Graphics)*, pp. 231–242, July 1998.

[16] C. Chang, G. Bishop, and A. Lastra, "LDI tree: A hierarchical representation for image-based rendering," *Proc. of SIGGRAPH (ACM Trans. Graphics),* pp. 291–298, Aug. 1999.

[17] L. McMillan and G. Bishop, "Plenoptic modeling: An image-based rendering system," *Proc. of SIGGRAPH (ACM Trans. Graphics)*, pp. 39–46, Aug. 1995.

[18] P.E. Debevec, Y. Yu, and G. Borshukov, "Efficient view-dependent image-based rendering with projective texture-mapping," *Proc. of Eurographics Workshop on Rendering*, pp. 150–116, 1998.

[19] ISO/IEC JTC1/SC29/WG11 and ITU-T Q6/SG16, "Joint multiview video model (JMVM) 5.0," Doc. JVT-X207, July 2007.

[20] ISO/IEC JTC1/SC29/WG11, "Proposal on standardization of free viewpoint TV (FTV)," Doc. M13612, July 2006.

[21] ISO/IEC JTC1/SC29/WG11, "Proposal on requirements for FTV," Doc. M14417, Apr. 2007.

[22] ISO/IEC JTC1/SC29/WG11, "Preliminary FTV model and requirements," Doc. N9168, July 2007.

[23] S.C. Chan, H.Y. Shum, and K.T. Ng, "Image-based rendering and synthesis," *Proc. of IEEE Signal Processing Magazines*, pp. 22–33, Nov. 2007.

[24] M. Levoy and P. Hanrahan, "Light field rendering," *Proc. of SIGGRAPH (ACM Trans. Graphics)*, pp. 31–42, Aug. 1996.

[25] S.J. Gortler, R. Grzeszczuk, R. Szeliski, and M.F. Cohen, "The lumigraph," *Proc. of SIGGRAPH (ACM Trans. Graphics)*, pp. 43–54, Aug. 1996.

[26] M. Tanimoto, "FTV (Free Viewpoint Television) creating ray-based image engineering," *Proc. of ICIP2005*, vol.2, pp. 25–28, 2005.

[27] M. Droese, T. Fujii, and M. Tanimoto, "Ray-Space interpolation based on filtering in disparity domain," *Proc. of 3D Conference 2004*, pp. 213–216, Tokyo, Japan, June 2004.

[28] ISO/IEC JTC1/SC29/WG11, "Description of exploration experiments in FTV," Doc. N9230, July 2007.

[29] Z. Wang, A. C. Bovik, H. R. Sheik, E. P. Simoncelli, "Image quality assessment: From error visibility to structural similarity, *Proc. of IEEE Transaction on Image Processing* vol. 13, no. 4, pp. 600–612, 2004.

[30] F. Xiao, "DCT-based video quality evaluation," *Final Project for EE392J Stanford Univ*. 2000.

[31] MSU Video Quality Measurement Tool. Available: http://compression.ru/video/quality_measure/

[32] A. Fusiello, "Uncalibrated euclidean reconstruction: a review," *proc. of Image and vision computing* vol. 18, pp. 555–563, 2000.

[33] E. Trucco and A. Verri, *Introductory Techniques for 3D Computer Vision*, Upper Saddle River, NJ: Prentice-Hall, 1998.

[34] R.Hartley and A.Zisserman, *Multiple View Geometry in Computer Vision*, Cambridge University Press, UK, 2000.

[35] J. A. Bangham and S. Marshall, "Image and signal processing with mathematical morphology," *Proc. of Electronics & Communication Engineering Journal*, pp.117–128, June 1998.

[36] MSR 3D video Sequences. Available: http://www.research.microsoft.com/vision/ImageBasedRealities/3DVideoDownload/.

[37] C. J. van den Branden Lambrecht and O.Verscheure, "Perceptual quality measure using a spatio-temporal model of the human visual system," *Proc. of SPIE*, vol. 2668, pp. 450–461, 1996.

[38] ISO/IEC JTC1/SC29/WG11, "Improvement of depth map estimation and view synthesis," Doc. M15090, Jan. 2008.

[39] U. Fecker, M. Barkowsky, and A. Kaup, "Improving the prediction efficiency for multi-view video coding using histogram matching," *Proc. of ICIP 2007*.

[40] A. Telea, "An image inpainting technique based on the fast marching method," *Proc. of Journal of Graphics Tools*, vol.9, no.1, pp.25–36, 2004.

[41] ISO/IEC JTC1/SC29/WG11, "Reference Softwares for Depth Estimation and View Synthesis," Doc. M15377, Apr. 2008.